Monthly Notices
of the
ROYAL ASTRONOMICAL SOCIETY

MNRAS **453,** 1489–1502 (2015) doi:10.1093/mnras/stv1722

Intrinsic instrumental polarization and high-precision pulsar timing

G. Foster,[1,2]★ A. Karastergiou,[1,2,3] R. Paulin,[2] T. D. Carozzi,[4] S. Johnston[5] and W. van Straten[6]

[1]*Department of Physics and Electronics, Rhodes University, PO Box 94, Grahamstown 6140, South Africa*
[2]*Sub-Department of Astrophysics, University of Oxford, Denys Wilkinson Building, Keble Road, Oxford OX1 3RH, UK*
[3]*Physics Department, University of the Western Cape, Cape Town 7535, South Africa*
[4]*Department of Earth & Space Sciences, Chalmers University of Technology, Onsala Space Observatory, SE-43992 Onsala, Sweden*
[5]*CSIRO Astronomy and Space Science, PO Box 76, Epping, NSW 1710, Australia*
[6]*Centre for Astrophysics and Supercomputing, Swinburne University of Technology, Hawthorn, VIC 3122, Australia*

Accepted 2015 July 27. Received 2015 July 21; in original form 2015 May 22

ABSTRACT

Radio telescopes are used to accurately measure the time of arrival (ToA) of radio pulses in pulsar timing experiments that target mostly millisecond pulsars (MSPs) due to their high rotational stability. This allows for detailed study of MSPs and forms the basis of experiments to detect gravitational waves. Apart from intrinsic and propagation effects, such as pulse-to-pulse jitter and dispersion variations in the interstellar medium, timing precision is limited in part by the following: polarization purity of the telescope's orthogonally polarized receptors, the signal-to-noise ratio of the pulsar profile, and the polarization fidelity of the system. Using simulations, we present how fundamental limitations in recovering the true polarization reduce the precision of ToA measurements. Any real system will respond differently to each source observed depending on the unique pulsar polarization profile. Using the profiles of known MSPs, we quantify the limits of observing system specifications that yield satisfactory ToA measurements, and we place a practical design limit beyond which improvement of the system results in diminishing returns. Our aim is to justify limits for the front-end polarization characteristics of next-generation radio telescopes, leading to the Square Kilometre Array.

Key words: instrumentation: polarimeters – pulsars: general – radio continuum: general.

1 INTRODUCTION

Any dual-polarization polarimeter is characterized by a degree of polarization purity, i.e. the cross-polarization between orthogonal feeds, and the extent to which calibration can be used to retrieve accurate polarization information. In this paper, we examine how both of these limitations affect pulsar ToA measurements, especially in the case of MSPs. We do this by simulating ToA measurements through a sampling of the signal-to-noise ratio (S/N), calibration error, and intrinsic polarization leakage parameter space. Intrinsic polarization leakage includes the apparent leakage between orthogonal receptors due to differential receptor gains, in addition to the cross-coupling between receptors, which is typically thought of as 'polarization leakage'.

Simulations are used, as it is difficult to analytically quantify the effects of calibration error, integration time, and intrinsic polarization leakage in a general form. The ToA measurement error depends on the ability to observe pulsar profiles with high fidelity. By profile, we mean the stable average shape of the radio pulse of a given pulsar and its polarization properties. We perform our analysis using profiles from the 20 MSPs in Manchester et al. (2013).

A fundamental limit to any ToA measurement is the design of the polarimeter feeds, which is set by the telescope specifications. As pulsar timing is a key science project for Square Kilometre Array (SKA), see Janssen et al. (2015) and Cordes et al. (2004), it is important to consider the science limitations set during the design process. The decimetre wavelength band, where pulsars are typically observed for timing, will be covered by both dishes and aperture arrays (AAs). The analysis presented here applies to both telescope types.

For the design of the feeds, we need to consider the capacity of any dish or AA to produce data from which the true polarization of a signal can be recovered. For example, the full polarization description of an incoming signal can never be recovered by a single dipole, no

★ E-mail: griffin.foster@gmail.com

matter how good the calibration procedure is. On more realistic systems, there is a fundamental limitation in recovering the polarization state due to differential gains between orthogonal receptors. These differential gains coupled with noise in the system result in measurement errors which cannot be corrected via any currently used calibration procedure. This affects all ToA measurement methods. For total intensity (e.g. Taylor 1992) timing methods, i.e. the determination of a ToA through cross-correlation of a total power template, this is an effect in addition to calibration error. Techniques such as the invariant interval (Britton 2000) and matrix template matching (van Straten 2006) methods, despite being largely independent of polarization calibration error, are also affected.

The remainder of this introduction covers the relevant Jones and Mueller mathematical formalisms necessary to describe intrinsic polarization leakage. In Section 2 we describe the simulation setup and the strategy for exploring the relevant parameter space, how the simulated observations are generated, and the methods for determining the ToA. Results are presented in Section 3. Discussion of the results and the implications for current and future telescopes are presented in Section 4.

1.1 Intrinsic polarization leakage in Jones and Mueller formalism

We are interested in describing the intrinsic polarization leakage of a linear feed, dual-polarization system as this is a typical design for single pixel feeds and phased arrays such as phased-array feeds (PAFs) and AAs used for pulsar timing. Intrinsic polarization leakage can be described with the mathematical structure developed for the radio interferometer measurement equation (RIME) presented in Hamaker, Bregman & Sault (1996) and Smirnov (2011a). Additionally, the RIME can be extended to phased arrays where, to first order, the formed beam is a linear combination of the individual element beams; a full description would also include element mutual coupling terms. Jones matrix formalism is useful to frame the RIME in terms of instrumentation and environmental effects on an electromagnetic signal. The Mueller matrix formalism, which is used in our simulations, is useful in interpreting the RIME in terms of detected power, represented by the Stokes parameters of the signal.

In Jones formalism, transformations are applied to an input electromagnetic signal to produce the observed signal. The transformation from the complex electromagnetic sky Jones vector $\boldsymbol{e}$ to the observed voltage Jones vector $\boldsymbol{v}$ is

$$\boldsymbol{v} = \mathbf{J}_{\rm sys}\boldsymbol{e}, \tag{1}$$

where $\mathbf{J}_{\rm sys}$ is the total system Jones matrix representation which is constructed out of multiple linear Jones transformations, each of which can have dependence on time, observing frequency, and source direction (Smirnov 2011b). In the scope of this paper, we are interested in the effect of intrinsic polarization leakage. The polarization leakage matrix $\mathbf{D}$ is usually defined as a direction-independent Jones matrix with the direction-dependent polarization leakage components incorporated into the primary beam matrix $\mathbf{E}$. For this work, we are not focusing on the primary beam direction-dependent sensitivity, but only the potentially direction-dependent polarization leakage; thus, for phased arrays we are defining $\mathbf{D}$ to also include the direction-dependent polarization leakage

$$\mathbf{D} = \begin{pmatrix} 1 & d_{p\rightarrow q}(\nu,\theta,\phi) \\ -d_{q\rightarrow p}(\nu,\theta,\phi) & 1 \end{pmatrix}, \tag{2}$$

where (θ, ϕ) are reference frame-dependent position angles. In equation (2), $d_{p\rightarrow q}$ is the intrinsic leakage of feed p into feed q. In feed design, the off-diagonal terms are minimized. Ideally, they are zero. For phased arrays, however, projection effects will cause $\mathbf{D}$ to vary with observing direction.

We can then define an explicit RIME for our dish and phased array systems as

$$\mathbf{J}_{\rm sys,dish} = \mathbf{B}(\nu)\mathbf{G}(t)\mathbf{C}\mathbf{D}(\nu) \tag{3a}$$

$$\mathbf{J}_{\rm sys,PA} = \sum_{i=1}^{n} \mathbf{W}_i(\nu,\theta,\phi)\mathbf{B}_i(\nu)\mathbf{G}_i(t)\mathbf{C}_i\mathbf{D}_i(\nu,\theta,\phi), \tag{3b}$$

where $\mathbf{B}$ is the frequency-dependent bandpass structure and $\mathbf{G}$ is the time-dependent electronic gain. $\mathbf{B}$ and $\mathbf{G}$ are diagonal matrices. The idealized nominal feed configuration $\mathbf{C}$ is a coordinate transform from the sky to observing frame. For a single pixel feed, on axis observation, $\mathbf{D}$ has no direction dependence and can be simplified to $\mathbf{D}(\nu)$.

For a phased array, the $\mathbf{J}_{\rm sys}$ is the weighted sum over all n elements of the array, where $\mathbf{W}_i$ are the complex weights to shape the array beam pattern to 'point' in a direction. For a PAF, the direction dependence of $\mathbf{D}$ will be relative to the dish pointing centre. For an AA, the direction dependence of $\mathbf{D}$ will be relative to the direction of boresight, usually zenith.

Jones formalism is useful for understanding the instrumental effects on a signal. For our simulation, however, we use pulsar profiles described as Stokes vectors, for which Mueller matrices are used to perform operations. Using the notation from Hamaker et al. (1996), any Jones matrix $\mathbf{J}$ can be transformed to a corresponding Mueller matrix $\mathbf{M}$ by use of the Kronecker product,

$$\mathbf{M} = \mathbf{S}^{-1}(\mathbf{J}\otimes\mathbf{J}^{*})\mathbf{S}, \tag{4}$$

where $\mathbf{S}$ and $\mathbf{S}^{-1}$ are the conversion matrices to transform between Stokes parameters and the brightness coherency vector. For reference they are presented below:

$$\mathbf{S} = \frac{1}{2}\begin{pmatrix} 1 & 1 & 0 & 0 \\ 0 & 0 & 1 & i \\ 0 & 0 & 1 & -i \\ 1 & -1 & 0 & 0 \end{pmatrix} \tag{5}$$

$$\mathbf{S}^{-1} = \begin{pmatrix} 1 & 0 & 0 & 1 \\ 1 & 0 & 0 & -1 \\ 0 & 1 & 1 & 0 \\ 0 & -i & i & 0 \end{pmatrix}. \tag{6}$$

Using equation (4) the feed-error matrix $\mathbf{D}$ can be converted to a Mueller form $\mathbf{D}_{\rm M}$ (equation 7). Each element of which can be directly computed using $\mathbf{M}_{i,j} = \frac{1}{2}\,\mathrm{tr}(\boldsymbol{\sigma}_i\,\mathbf{J}\,\boldsymbol{\sigma}_j\,\mathbf{J}^{\dagger})$, where $\boldsymbol{\sigma}_i$ is the ith Pauli matrix. In this form, the (i, j)th element can be understood as the response of the ith output to the jth input:

$$\mathbf{D}_{\rm M} = \begin{pmatrix} 1+\frac{1}{2}(|d_{p\to q}|^2+|d_{q\to p}|^2) & \frac{1}{2}(|d_{p\to q}|^2+|d_{q\to p}|^2) & \mathrm{Re}[d_{p\to q}-d_{q\to p}] & \mathrm{Im}[d_{p\to q}+d_{q\to p}] \\ \frac{1}{2}(|d_{p\to q}|^2-|d_{q\to p}|^2) & 1-\frac{1}{2}(|d_{p\to q}|^2-|d_{q\to p}|^2) & \mathrm{Re}[d_{p\to q}+d_{q\to p}] & -\mathrm{Im}[d_{p\to q}-d_{q\to p}] \\ \mathrm{Re}[d_{p\to q}-d_{q\to p}] & -\mathrm{Re}[d_{p\to q}+d_{q\to p}] & 1-\mathrm{Re}[d_{p\to q}d^*_{q\to p}] & \mathrm{Im}[d_{p\to q}d^*_{q\to p}] \\ \mathrm{Im}[d_{p\to q}+d_{q\to p}] & -\mathrm{Im}[d_{p\to q}-d_{q\to p}] & \mathrm{Im}[d_{p\to q}d^*_{q\to p}] & 1+\mathrm{Re}[d_{p\to q}d^*_{q\to p}] \end{pmatrix}. \tag{7}$$

1.2 Polarimeter performance metric

The polarization leakage of a dual-feed receiver is quantified by using cross-polarization ratio (XPR) metrics (IEEE 1998). In Carozzi & Woan (2011), a new XPR, the polarimeter intrinsic cross-polarization ratio (IXR), was introduced. XPRs are used as metrics for radio communication feeds where the polarization of both the source and receiver is known. Thus, an XPR can vary by choice of coordinate system (Carozzi & Woan 2011). The IXR is an XPR which is invariant under coordinate transform. This makes the IXR ideal for a radio astronomical polarimeter as there is no preferred sky coordinate frame. The IXR in Jones formalism is defined as

$$\mathrm{IXR_J} \equiv \left(\frac{g_{\max}+g_{\min}}{g_{\max}-g_{\min}}\right)^2, \tag{8}$$

where $g_{\max}$ and $g_{\min}$ are the maximum and minimum amplitude gains of the polarimeter when using singular value decomposition (SVD) to decompose the system Jones matrix $\mathbf{J}_{\rm sys}$. The SVD theorem (equation 9) states that any Jones matrix $\mathbf{J}$ can be decomposed into two unitary transforms $\mathbf{U}, \mathbf{V}^{\dagger}$ and one diagonal transform matrix Σ:

$$\mathbf{J} = \mathbf{U}\Sigma\mathbf{V}^{\dagger} = \mathbf{U}\begin{pmatrix} \sigma_{\max} & 0 \\ 0 & \sigma_{\min} \end{pmatrix}\mathbf{V}^{\dagger}. \tag{9}$$

Given a noise input signal $\boldsymbol{e}$, the sensitivity to change in $\boldsymbol{v}$ from equation (1) is measured by the *matrix condition number* $\mathrm{cond}_2(\mathbf{J}) \equiv \kappa(\mathbf{J}) = \frac{\sigma_{\max}}{\sigma_{\min}}$, where $\sigma_{\max}$ and $\sigma_{\min}$ are the maximum and minimum singular values. An *ill-conditioned* matrix, one with a condition number much larger than 1, will cause an increase in the error of $\boldsymbol{v}$ with respect to the error of $\boldsymbol{e}$. Conversely, a *well-conditioned* matrix, one with a condition number close to 1, will transform $\boldsymbol{e}$ into $\boldsymbol{v}$ with minimal effect on the error.

Carozzi & Woan (2011) show that by setting the maximum and minimum amplitude gains to be equal to the maximum and minimum singular values ($\sigma_{\max} = g_{\max}$ and $\sigma_{\min} = g_{\min}$), there is always an orthonormal choice of coordinate systems for the sky and the channels that gives $\mathbf{J}'$ from $\mathbf{J}$ such that the feed-error matrix takes the form

$$\mathbf{J}' = \frac{g_{\max}+g_{\min}}{2}\begin{pmatrix} 1 & 1/\sqrt{\mathrm{IXR_J}} \\ 1/\sqrt{\mathrm{IXR_J}} & 1 \end{pmatrix}. \tag{10}$$

The $\mathrm{IXR_J}$ is in units of power, and equation (10) has components of $\sqrt{\mathrm{IXR_J}}$ as a Jones matrix acts as an operation on an electric field vector. Intrinsic polarization leakage can be seen as differential gains or 'canonical' polarization leakage depending on the basis. The condition number can thus be related back to the intrinsic polarization leakage. That is $d_{p\to q} = -d_{q\to p} = \frac{\kappa(\mathbf{J})+1}{\kappa(\mathbf{J})-1}$ with a normalization factor of $\frac{\kappa(\mathbf{J})+1}{2\kappa(\mathbf{J})}$. Redefining the $\mathrm{IXR_J}$ in terms of the condition number, equation (8) becomes

$$\mathrm{IXR_J} = \left(\frac{\kappa(\mathbf{J})+1}{\kappa(\mathbf{J})-1}\right)^2. \tag{11}$$

This is a crucial quantity which represents a fundamental limit in our ability to recover the true signal. This limit is independent of the polarization calibration.

The IXR is conceptually equivalent to the *polconversion* (Hamaker 2000) and Lorentz boost (Britton 2000) transformations that have been employed in previous works based on quaternions and geometric algebra, respectively. For example, where β is the velocity parameter that describes a Hermitian Jones matrix in equation 11 of Britton (2000), $\kappa(\mathbf{J}) = e^{2\beta}$ and $\mathrm{IXR_J} = \coth^2(\beta)$. These equations enable meaningful comparisons between the results presented in this work and the notation employed in some previous studies (e.g. van Straten 2013).

To understand how the condition number, and by extension the IXR, affects an observation, we can look at how the true sky vector $\boldsymbol{e}$ is determined. To obtain an estimate of the true Jones sky vector $\hat{\boldsymbol{e}}$ from the observed Jones vector $\boldsymbol{v}$, the system Jones matrix $\mathbf{J}_{\mathrm{sys}}$ must be determined and inverted (equation 12) via calibration

$$\hat{\boldsymbol{e}} = \mathbf{J}_{\mathrm{sys}}^{-1}\boldsymbol{v}, \tag{12}$$

where $\hat{\boldsymbol{e}}$ is an estimate of $\boldsymbol{e}$ due to multiple compounding effects. First, in the measurement of $\boldsymbol{v}$, there is a limit in precision due to noise. Secondly, $\mathbf{J}_{\mathrm{sys}}$ is not perfectly known, but is an estimate based on modelling and calibration. Finally, the condition of the components of $\mathbf{J}_{\mathrm{sys}}$ determine how the errors in measurement affect the estimation of $\hat{\boldsymbol{e}}$. For an ill-conditioned $\mathbf{J}_{\mathrm{sys}}$, a small error in $\boldsymbol{v}$ will result in a large error in estimated sky vector $\hat{\boldsymbol{e}}$ compared to the true sky vector $\boldsymbol{e}$. An ill-conditioned $\mathbf{J}_{\mathrm{sys}}$ matrix will lead to a noisy estimate of $\boldsymbol{e}$, no matter how well known $\mathbf{J}_{\mathrm{sys}}$ is, due to the inherent noise in the measurement of $\boldsymbol{v}$. As the conditioning of the $\mathbf{J}_{\mathrm{sys}}$ improves, so too does $\hat{\boldsymbol{e}}$ more accurately describe $\boldsymbol{e}$.

By definition $\kappa(\mathbf{J}) \geq 1$. Ideally, there is no intrinsic polarization leakage between feeds, i.e. the matrix is perfectly conditioned $g_{\max} = g_{\min} \Rightarrow \kappa(\mathbf{J}) = 1$ and the $\mathrm{IXR_J} \rightarrow \infty$. That is, the two receptors are completely orthonormal. If there is intrinsic leakage between the two feeds, then $g_{\max} > g_{\min} \Rightarrow \kappa(\mathbf{J})$ increases and the $\mathrm{IXR_J}$ decreases. In the worst case (e.g. where the two feeds are perfectly coupled, or one receptor's sensitivity goes to 0), then $g_{\min} \rightarrow 0 \Rightarrow \kappa(\mathbf{J}) \rightarrow \infty$ and the $\mathrm{IXR_J} \rightarrow 1$. Since the $\mathrm{IXR_J}$ is a measure of feed response, it is common to use decibel (dB) units, $\mathrm{IXR_{J,\,dB}} = 10\log_{10}(\mathrm{IXR_J})$.

We can also consider the IXR in terms of Mueller matrices. Carozzi & Woan (2011) connect the IXR to Mueller matrices by showing $\kappa(\mathbf{M}) = \kappa^2(\mathbf{J})$. This relation is used to show that the IXR in Mueller formalism is

$$\mathrm{IXR_M} = \frac{\kappa(\mathbf{M}) + 1}{\kappa(\mathbf{M}) - 1} = \frac{1 + \mathrm{IXR_J}}{2\sqrt{\mathrm{IXR_J}}} \tag{13}$$

which provides a useful metric for measuring the impact of instrumental polarization on the Stokes parameters, especially in the case of impure transformations with no corresponding Jones matrix.

An example of the variation in $\mathrm{IXR_J}$ across the field of view (FoV) of a simple dipole element is shown in Fig. 1. The $\mathrm{IXR_J}$ is maximized (70 dB) in the direction of zenith, but rises when observing away from boresight. The low-$\mathrm{IXR_J}$ structure [(0°, 180°) and (90°, 270°) axes] is along the 45° line between the two orthogonal receptors. The variation in $\mathrm{IXR_J}$ across the FoV also depends on observing frequency.

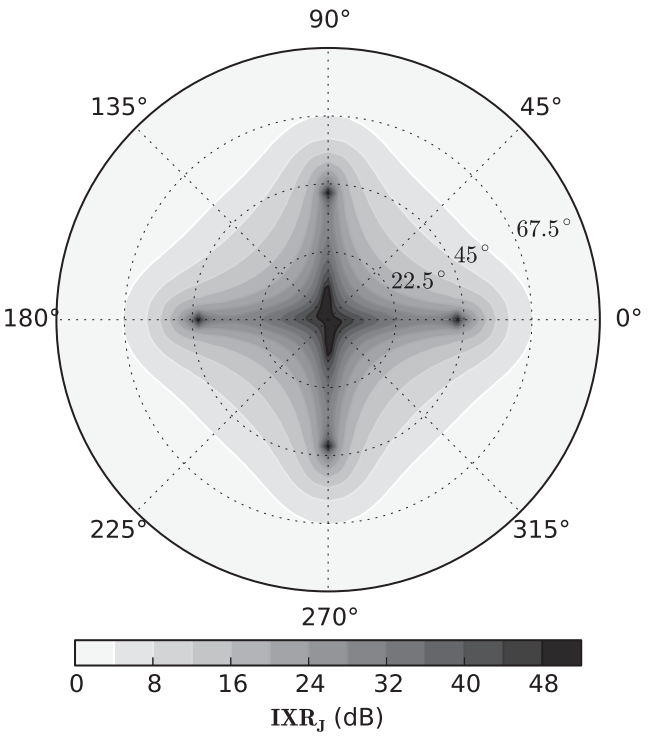

Figure 1. $\mathrm{IXR_J}$ of a simple 'all-sky' element based on the Precision Array for Probing the Epoch of Reionization dipole beam model at 130 MHz. The orthogonal dipoles are oriented along the (45°, 225°) and (135°, 315°) axes.

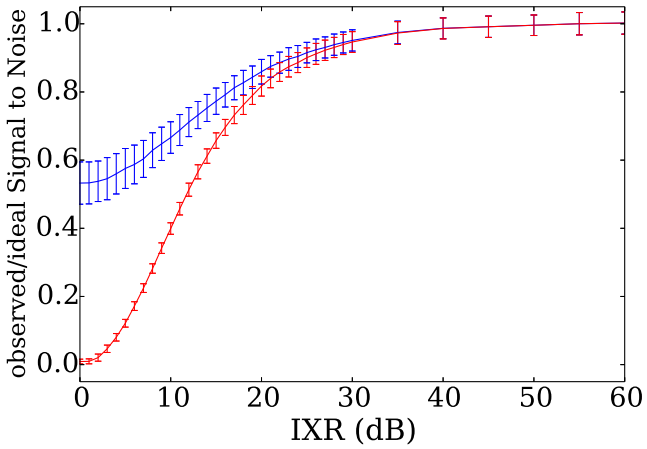

Figure 2. The average observed S/N of J1603−7202 as a fraction of the ideal S/N for a range of IXR values using 'gain' (blue solid) and 'full' (red dashed) calibration methods described in Section 2.2.

Carozzi, Woan & Maaskant (2009) and Sutinjo & Hall (2013) show that the $\mathrm{IXR}_{\mathrm{J,\,dB}}$ can vary between 0 and 66 dB across an AA depending on pointing direction and element design. For an idealized short dipole, the $\mathrm{IXR}_{\mathrm{J}}$ varies smoothly over the observable hemisphere. But for many feeds – such as Vivaldi-type, bow-tie, and narrow-band half-wavelength dipoles – sharp intrinsic polarization leakage structures form across the hemisphere. Figs 3 and 5 in Carozzi et al. (2009) show the $\mathrm{IXR}_{\mathrm{J}}$ over a hemisphere for short dipoles and Vivaldi-type elements. Figs 2 and 3 in Sutinjo & Hall (2013) show the $\mathrm{IXR}_{\mathrm{J}}$ across the FoV of an Murchison Widefield Array (MWA) bow-tie element. These published values and maps provide insight into what range of $\mathrm{IXR}_{\mathrm{J}}$ to use in our simulations.

1.3 IXR and S/N

The error on a ToA measurement is, in general, a function of the S/N of a given observation. By S/N, we hereby refer to the peak pulse value in the Stokes *I* profile to the standard deviation of the off-pulse signal. Under ideal circumstances, the S/N increases with the square root of integration time. For a polarized source, instrumental intrinsic polarization leakage will result in a lower observed S/N compared to the ideal S/N, i.e. that obtained from a system with no intrinsic polarization leakage, for a given amount of integration. The blue solid line in Fig. 2 shows the fractional observed S/N compared to the ideal S/N as a function of the IXR for J1603−7202. The red dashed line shows how using the inverse of a poorly conditioned matrix for calibration amplifies the noise in the measured profile. This will be discussed further in Section 2. All the simulated pulsars have a similar response. An effect of a low IXR is the introduction of a differential gain between feeds. As the IXR goes to 0, the receiver system becomes effectively blind to one polarization; thus, the observed S/N is approximately half (blue solid line) that of the ideal S/N in the limit $\mathrm{IXR} \rightarrow 0$. When calibration is applied, not only is there a differential gain effect, but the inversion of the ill-conditioned matrix will significantly degrade the S/N of any profile (red dashed line). The ideal S/N is achieved only in the limit as $\mathrm{IXR} \rightarrow \infty$, and there is a one-to-one correspondence with integration time. A reference integration time of $\tau_{\mathrm{int}} = 1$ is defined as the time it would take to build up an ideal S/N of 1000. All integration time values quoted in this paper are a fraction of this reference integration time. The relationship between τ_{int} and ideal S/N $\mathrm{SN_I}$ is

$$\tau_{\mathrm{int}} = \left(\frac{\mathrm{SN_I}}{1000}\right)^2.$$

2 THE SIMULATIONS

We have performed simulations with the goal to quantify the effect of intrinsic polarization leakage on pulsar ToA measurements. We have sampled the three-dimensional parameter space that includes the $\mathrm{IXR}_{\mathrm{J}}$, ideal pulse profile S/N, and calibration error, which covers current telescope measurements and future telescope specifications. For each point in the sampled parameter space, 'observed' profiles are generated for 500 epochs, by modifying a template profile with the appropriate Mueller matrices. For every epoch, we stochastically generate the $\mathbf{J}_{\mathrm{sys}}$ Jones matrix, and the corresponding Mueller matrix $\mathbf{M}_{\mathrm{sys}}$, for a given intrinsic polarization leakage. The form of this matrix is described in Section 2.2. The observed profile is then calibrated by multiplying by the inverse of the system Mueller matrix with additive random calibration errors.

A ToA is determined at each of the 500 epochs, using a standard timing method (Section 2.3) included in PSRCHIVE (Hotan, van Straten & Manchester 2004; van Straten, Demorest & Oslowski 2012). In a normal pulsar timing experiment, a model would then be fitted to the ToA measurements using TEMPO2 (Hobbs, Edwards & Manchester 2006), and the goodness of the model would be measured by the root mean square (rms) of the timing residuals. Since we are using a simple model of an isolated, stable pulsar of constant period, this rms represents the ideal rms for a given set of parameters.

In the following, we give further details of the steps of the simulation.

2.1 Pulse profiles

We performed our simulations using profiles based on the mean pulse profiles of 20 well-studied MSPs from the Parkes Pulsar Timing Array (Manchester et al. 2013). It is not our intention to reproduce the results of that work. We use these MSPs as they cover a wide range of profile and polarization structures, and perform our simulations to much higher S/Ns than is possible with current experiments.

A high-S/N version of each reference profile was generated by applying a rolling Hann filter with a width of ∼1 per cent of the profile. This has the effect of removing high-frequency components and reduces the amplitude (up to a few per cent) of narrow profile structures. This was done in order to avoid very low uncertainties in our TOA measurements due to the presence of the same high-frequency structures in the templates and the simulated noisy data. Though we retain the pulsar names, by applying this filter, the new profiles are approximations to the original profiles and are meant only to be a representative set of profile structures. The low-frequency components that remain may cause our uncertainties to be systematically lower than real timing experiments for these pulsars; however, this effect is consistent across our simulations and therefore does not affect our final result.

The ideal profiles are then used to generate imperfect profiles at each epoch using the process described in Section 2.2. These profiles were also used as the template profiles when performing timing. The first and third columns of Figs 6 and 7 at the end of this paper are the Stokes parameters of the ideal profiles.

2.2 Simulated observations

Our simulated observations produce an estimated sky Stokes vector $\hat{\boldsymbol{e}}^S$ for a given pulsar per epoch by estimating the system Mueller matrix, including calibration error, intrinsic polarization leakage, and S/N parameters. Fig. 3 shows the stages to arrive at an example $\hat{\boldsymbol{e}}^S$.

The explicit RIMEs defined in equation (3) can be simplified for the simulations. By using the mean profile, we are making the simplification that the bandpass $\mathbf{B}$ and time-varying $\mathbf{G}$ system gains have been solved for and applied to the observed signal. Thus, $\mathbf{B}$ and $\mathbf{G}$ are unity diagonal matrices. We include a polarization calibration error term $\Delta\mathbf{J}$ into our system to simulate the effect of imperfect calibration of $\mathbf{B}$ and $\mathbf{G}$. The nominal feed matrix $\mathbf{C}$ is a telescope-specific basis transform, and will not affect the IXR as it is a coordinate-independent metric (i.e. $\mathrm{IXR_C} = \infty$). Thus, the polarization leakage matrix $\mathbf{D}$ is the only matrix which will vary in our parameter space. In practice, $\mathbf{D}$ is a function of frequency, but as the profile is an average across a frequency band, so too is the IXR a frequency-averaged intrinsic polarization leakage.

To generate a simulated observed profile, we start by creating an intrinsic polarization leakage Jones matrix representation. We define the *polarization leakage* to be $1/\sqrt{\mathrm{IXR_J}}$; in decibel units the intrinsic polarization leakage is $-\mathrm{IXR_{J,\,dB}}$. We have chosen this definition as polarization leakage is a common concept within the community. The IXR is a measure of both the cross-coupling between receiver feeds, which is typically thought of as 'polarization leakage', and the apparent leakage due to differential feed gains and thus is a more complete metric for 'polarization leakage' over previous definitions. A higher intrinsic polarization leakage implies that the two feeds are more coupled together than a lower intrinsic polarization leakage. To sample a broad range of intrinsic polarization leakage values, we sample the space 0 to −30 dB, where the upper limit of 0 dB is effectively blind to one polarization, such as a single polarization receiver. The intrinsic polarization leakage sample space in IXR notation is $1 \geq 1/\sqrt{\mathrm{IXR_J}} \geq 0.031$. By inverting equation (11), the condition number is related to the $\mathrm{IXR_J}$ as

$$\kappa(\mathbf{J}) = \frac{\sqrt{\mathrm{IXR_J}} + 1}{\sqrt{\mathrm{IXR_J}} - 1}. \tag{14}$$

For each run of the simulation with a given set of parameters, we construct a system Jones matrix $\mathbf{J}_{\mathrm{sys}}$ (equation 1) by generating a random complex matrix from a normal distribution ($\mu = 0$, $\sigma = 1$) for $\mathbf{D}$. All other matrices in $\mathbf{J}_{\mathrm{sys}}$ are simplified to unity matrices as discussed earlier in the section. The random matrix is decomposed using SVD (equation 9), and the singular values in Σ are replaced with those for the simulated IXR parameter. Without loss of generality, we normalize Σ using $\sigma_{\max} = g_{\max} = 1$. The normalized condition number becomes $\kappa(\mathbf{J}) = 1/g_{\min}$, and the system Jones matrix due to intrinsic polarization leakage becomes

$$\mathbf{J}_{\mathrm{sys}} = \mathbf{U}\Sigma\mathbf{V}^{\dagger} = \mathbf{U}\begin{pmatrix} 1 & 0 \\ 0 & \frac{1}{\kappa(\mathbf{J})} \end{pmatrix}\mathbf{V}^{\dagger}. \tag{15}$$

We use a random matrix as there is an infinite set of Jones matrices for a given IXR. The decomposition by SVD and reconstruction steps are to maintain the same scaling as with the calibration error Jones matrix.

For error in the polarization calibration, we use a sample space starting at the ideal perfect calibration (0 per cent) up to 15 per cent calibration error. This calibration error represents the imperfect measurement of $\mathbf{B}$ and $\mathbf{G}$, the inverse of which are applied to the observed signal to integrate the profile in both time and frequency. A calibration error matrix $\Delta\mathbf{J}$ is generated from a random normal complex distribution ($\mu = 0, \sigma = \mathrm{percenterror}/100$). The estimated system Jones matrix is $\hat{\mathbf{J}}_{\mathrm{sys}} = \mathbf{J}_{\mathrm{sys}} + \Delta\mathbf{J}$. This error parameter space covers a wide range of polarization calibration situations, although the typical calibration error is of the order of a few per cent (Han et al. 2009). In practice, the polarization calibration solution will also be affected by the IXR. We simulate this effect by using two different calibration techniques discussed later in this section. Additionally, this error does not include the potential error from approximating $\mathbf{D}$ based on beam modelling and observations that would be done in a real system. Using equation (4), $\mathbf{J}_{\mathrm{sys}}$ and $\hat{\mathbf{J}}_{\mathrm{sys}}$ are converted to their Mueller forms $\mathbf{M}_{\mathrm{sys}}$ and $\hat{\mathbf{M}}_{\mathrm{sys}}$.

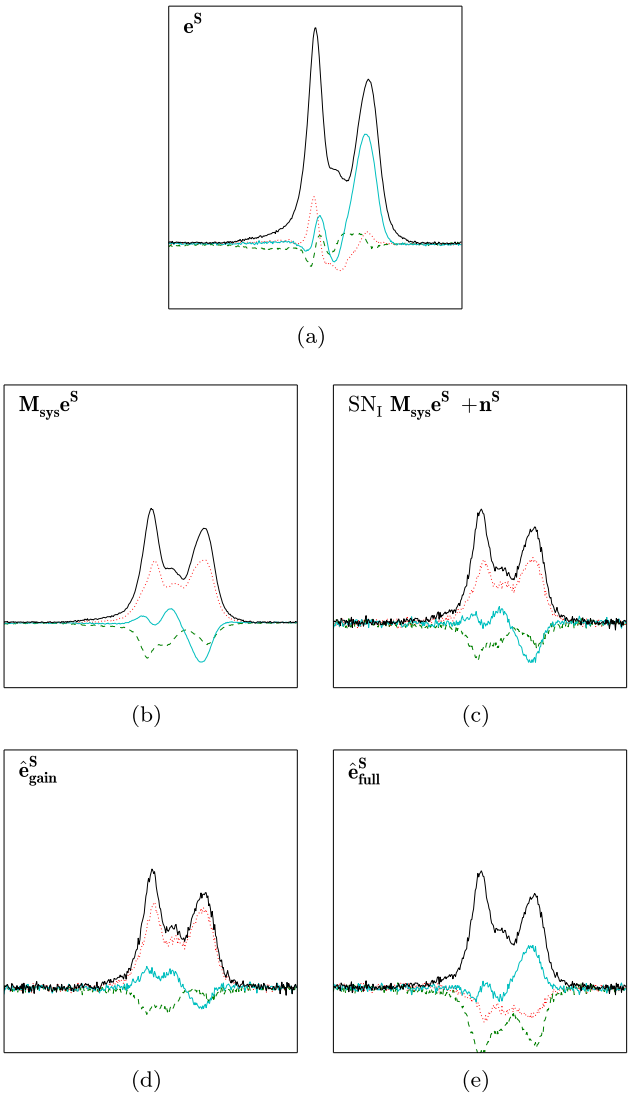

Figure 3. Stages of simulation for J1603−7202. Central third of pulse profile plotted. Stokes parameters: I (black solid), Q (green dashed), U (red dotted), and V (cyan solid). (a) True sky Stokes vector $\boldsymbol{e}^S$ of the pulsar profile. (b) True system Mueller matrix $\mathbf{M}_{\rm sys}$ with the condition number $\kappa(\mathbf{J})$ set for $\mathrm{IXR_{J,\,dB}} = 7$ dB applied to $\boldsymbol{e}^S$. (c) Added receiver noise for an $\mathrm{SN_I}$ of 100. (d) Estimated Stokes vector $\hat{\boldsymbol{e}}^S$ of the pulse profile used in timing experiment using 'gain' calibration with 20 per cent calibration error. (e) Estimated Stokes vector $\hat{\boldsymbol{e}}^S$ of the pulse profile used in timing experiment using 'full' calibration with 20 per cent calibration error.

To set the simulation S/N, we add a system noise component appropriate for the integration time of the simulated observation as described in Section 1.3. This is set by scaling the ideal profile $\boldsymbol{e}^S$, which has been normalized such that the Stokes I peak is unity, by a scalar $\mathrm{SN_I}$ value and adding a system noise Stokes vector $\boldsymbol{n}^S$ which is a set of real random values from a normal distribution ($\mu = 0, \sigma = 1$). The noise component $\boldsymbol{n}^S$ is a direction-independent effect. This is a practical approximation when the system noise is receiver noise dominated or when the sky noise is isotropic on the scale of the beam primary lobe. In the extreme case where all the system noise is direction dependent in the direction of the source, the effect on rms timing will only be a loss in S/N as seen in Fig. 2. As we will see in the following sections, the effect of direction-independent noise is to further degrade the timing solutions beyond the loss in S/N. For simplicity, we are using only direction-independent noise for the simulation.

An ideal S/N is set to be in the range $\sqrt{10^3}$ to $\sqrt{10^7}$ for our simulations, though we note that the observed S/N is reduced as the condition number increases, and thus the actual S/N is a function of IXR as shown in Fig. 2. The estimated Stokes vector $\hat{\boldsymbol{e}}^S$ of the observed pulsar is

$$\hat{\boldsymbol{e}}^S = \hat{\mathbf{M}}_{\rm sys}^{-1}(\mathrm{SN_I} \times \mathbf{M}_{\rm sys}\, \boldsymbol{e}^S + \boldsymbol{n}^S). \tag{16}$$

The inversion of $\hat{\mathbf{M}}_{\rm sys}$ is the calibration stage (equation 12). We have simulated two types of calibration. The first is a 'gain' calibration where we are only interested in solving the bandpass and electronic gain of the system, that is $\hat{\mathbf{J}}_{\rm sys} = \mathbf{BGC} + \Delta\mathbf{J} = \mathbf{I} + \Delta\mathbf{J}$, where $\mathbf{I}$ is the identity matrix. This is an ideal calibration solution where the gain terms can be solved for independently of any $\mathbf{D}$ effects, such as if using a known noise reference in a single dish system. The second type of calibration is a 'full' calibration where the $\mathbf{D}$ term is included, $\hat{\mathbf{J}}_{\rm sys} = \mathbf{BGCD} + \Delta\mathbf{J} = \mathbf{D} + \Delta\mathbf{J}$. This is a more realistic approach, as the IXR will affect any calibration solution. And, when performing

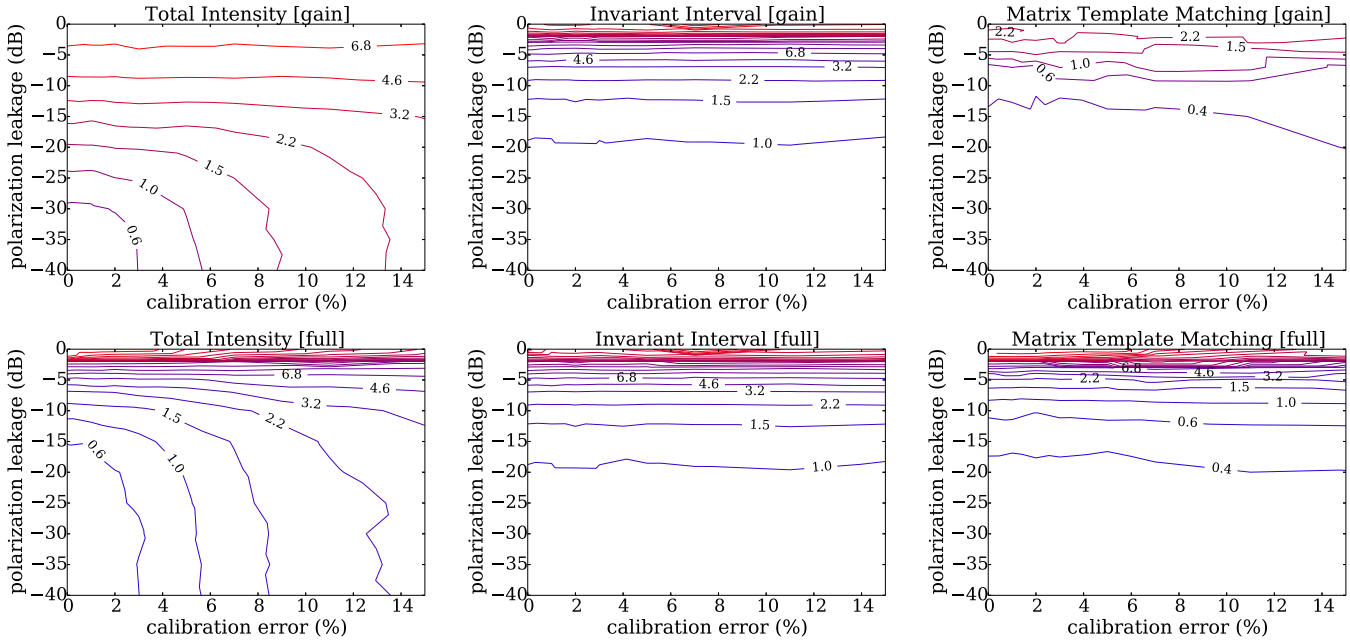

Figure 4. Contour plots of ToA rms noise (μs) from simulation of PSR J1603−7202 as a function of calibration error and intrinsic polarization leakage. The top row shows the effect of intrinsic polarization leakage on timing for the three methods when 'gain' calibration is applied. The bottom row is the same simulations but with 'full' calibration applied. There is a strong dependence on polarization calibration error when using the total intensity method. The solutions when using the invariant interval are effectively identical for both types of calibration. Matrix template matching outperforms the invariant interval method in both the calibrated and uncalibrated cases. An ideal SNR of 100 was used for these figures.

timing with an array, complex gain solutions are required to combine signals in phase by using a sky calibrator source or self-calibration. The calibratability of an array is a topic which should be studied in further work. Fig. 2 shows the effect of these two methods on observed S/N, independent of pulsar and ideal S/N. Examples of these types of calibration on the observed profile are shown in Figs 3(d) and (e). After a simulated $\hat{\boldsymbol{e}}^S$ is produced, a ToA is then determined with standard pulsar timing software. The effect of these calibration methods on timing will be shown in the following section. The simulation code is available as a git repository.[1]

2.3 Methods for TOA determination

For ToA measurements, three standard methods are used: total intensity (Taylor 1992), invariant interval (Britton 2000), and matrix template matching (van Straten 2006). These methods are included in `PAT`, from the PSRCHIVE package. For the total intensity method, each observed Stokes I profile is cross-correlated with the ideal template. The invariant interval technique uses all Stokes parameters in the form of a Lorentz 4-vector $(I^2 - Q^2 - U^2 - V^2)^{1/2}$. By including all Stokes parameters, complete information is used. However using the invariant form, the S/N decreases, leading to a less precise ToA determination compared to the intensity fitting, when the source is highly polarized or intrinsically weak (see van Straten 2013 for more information on this effect). Matrix template matching represents the profile in Jones notation and produces a ToA measurement while simultaneously solving for a calibration solution by transforming the template profile to the observed profile. In practice, the S/N requirements for timing often 'force' a pre-processing step of frequency and time averaging. This requires some prior level of polarization calibration, as described in the previous section, rendering the assumptions for matrix template matching no longer strictly valid, by introducing covariances between the Stokes parameters, especially for large polarization leakage.

Fig. 4 shows the ToA rms derived from the three timing methods used in simulations of the well-studied MSP J1603−7202. There is a strong dependence on polarization calibration error when using the total intensity timing method. Applying the 'full' calibration results in better timing solutions except in the high intrinsic polarization leakage region (>-5 dB), compared to using only the 'gain' calibration. We will use the 'full' calibration simulations for our total intensity results. The timing error, when using the invariant interval method, is effectively the same for both types of calibration.

For the matrix template matching method, there is a significant change in the ToA rms at high intrinsic polarization leakage between the two types of calibration. This is due to 'full' calibration introducing covariances between Stokes parameters, compared to just 'gain' calibration. Simulations using 'gain' calibration and timed with matrix template matching produce the best timing results for a given calibration error and intrinsic polarization leakage. We will present matrix template matching results using both types of calibration, but will focus our analysis on the 'full' calibration as it represents a more pragmatic result in terms of system calibration, especially when using an array for timing which requires multiple signals to be combined in phase.

[1] https://github.com/griffinfoster/pulsar-polarization-sims

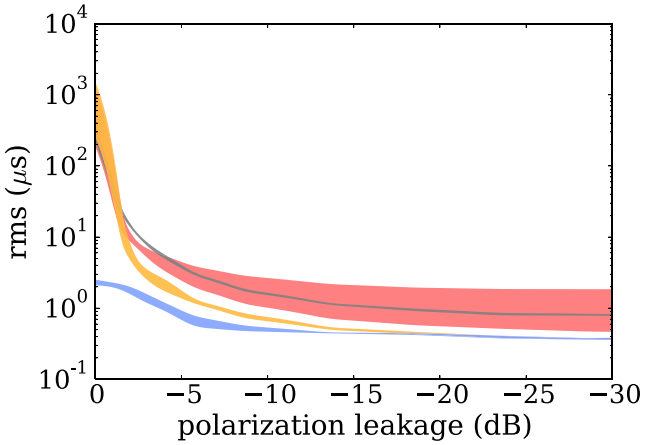

Figure 5. ToA rms noise for J1603−7202 as a function of intrinsic polarization leakage using the three timing methods: total intensity (red, no border), invariant interval (grey, dashed border), and matrix template matching (full calibration: orange, dotted border; gain calibration: blue, dot–dashed border). The width of the lines shows the effect polarization calibration error has on the ToA rms noise; a polarization calibration error from 0 to 15 per cent was used. These simulations use a fractional integration time of 0.01 which would produce an ideal S/N of 100.

In practice, total intensity and invariant interval are commonly used methods, whereas the matrix template matching method is more rarely used due to the difficulties in practical polarization calibration. However, as timing limits are pushed, matrix template matching will become necessary (van Straten 2013).

3 RESULTS

As polarization calibration error is not the focus of these simulations, we can compress the contour plots in Fig. 4 into a more concise and useful figure by collapsing the calibration error axis. Fig. 5 shows the bound range for each method on a single plot. The narrowness of the bounds for the invariant interval and matrix template matching show their independence from polarization calibration error. Plots of this style for all the simulated MSPs are shown at the end in Figs 6 and 7. These figures show that as the intrinsic polarization leakage decreases, so too do the timing residuals using all methods.

We have chosen to use the ToA rms noise as the metric for these results. This is a measure of the ToA scatter for the simulations. Using the average ToA uncertainty $\sigma_{\rm ToA}$ underestimates the error. As per equation 8.2 of Lorimer (2005) $\sigma_{\rm ToA} \simeq W/{\rm SN_o}$, where W is the pulse width and $\rm SN_o$ the observed S/N. In our simulation results, we see that the intrinsic polarization leakage affects timing results beyond a simple reduction of the S/N, producing poorer rms timing residuals compared to the average $\sigma_{\rm ToA}$ of the same simulated observations. In the limit ${\rm IXR_J} \rightarrow \infty$, the rms noise will reach $\sigma_{\rm ToA}$.

We computed the reduced χ^2 solution to measure the goodness of fit for each sample of the parameter space. When computing the χ^2 of the measured ToA against the expected ToA, the low intrinsic polarization leakage case results in a good fit, as would be expected. As the intrinsic polarization leakage increases, the fit degrades. Paradoxically, as the intrinsic polarization leakage increases to the highest values, the reduced χ^2 fit approaches 1. This is because $\sigma_{\rm ToA}$ grows exponentially large, and the error of the fit is within the limits of the ToA variance.

Although the diverse set of profiles we have simulated produce different results, seen in Figs 6 and 7, there are general trends we observe. All the simulations with the 'full' calibration profiles show exponentially increasing rms timing solutions as the intrinsic polarization leakage increases. Using only 'gain' calibration produces good timing results in this region, but is not as realistic as the 'full' calibration simulations.

Generally, using matrix template matching, with 'gain' or 'full' calibration, produces better timing solutions compared to other methods at all intrinsic polarization leakage values. For the majority of the 'gain' calibrated profiles, matrix template matching produces timing solutions that are only weakly dependent on intrinsic polarization leakage. It is worth noting that, for a few profiles, such as J1022+1001, matrix template matching of the 'full' calibration profile produces lower rms timing residuals than the 'gain' calibrated profile. This profile has highly polarized components, which are distorted by high intrinsic polarization leakage. At high intrinsic polarization leakage, the profiles with 'full' calibration result in high-rms timing residuals and dependence on polarization calibration error when using matrix template matching. However, at low intrinsic polarization leakage, both types of calibration converge to a similar timing solution.

The results from using the invariant interval method are consistent across all profiles. In a few cases, for example J1744−1134 and J1824−2452, the invariant interval method significantly underperforms compared to the other methods. Both these pulsars are highly polarized; therefore, in the invariant interval, the power in Stokes I is almost entirely cancelled out by the other Stokes parameters.

Timing solutions with the total intensity method have a notable dependence on the polarization calibration error. Plotting the bound regions as individual lines for different polarization calibration errors in Fig. 8, there is a polarization leakage point (e.g. for PSR J1603−7202 it is around −4 dB), after which systems with higher polarization calibration error produce better timing solutions than an ideally calibrated system. This is true for all MSP profiles used in our simulation, though transition points vary between −3 and −7 dB. In this region of the parameter space, this counter-intuitive effect comes about because the error-free calibrator transformation also has high intrinsic leakage and

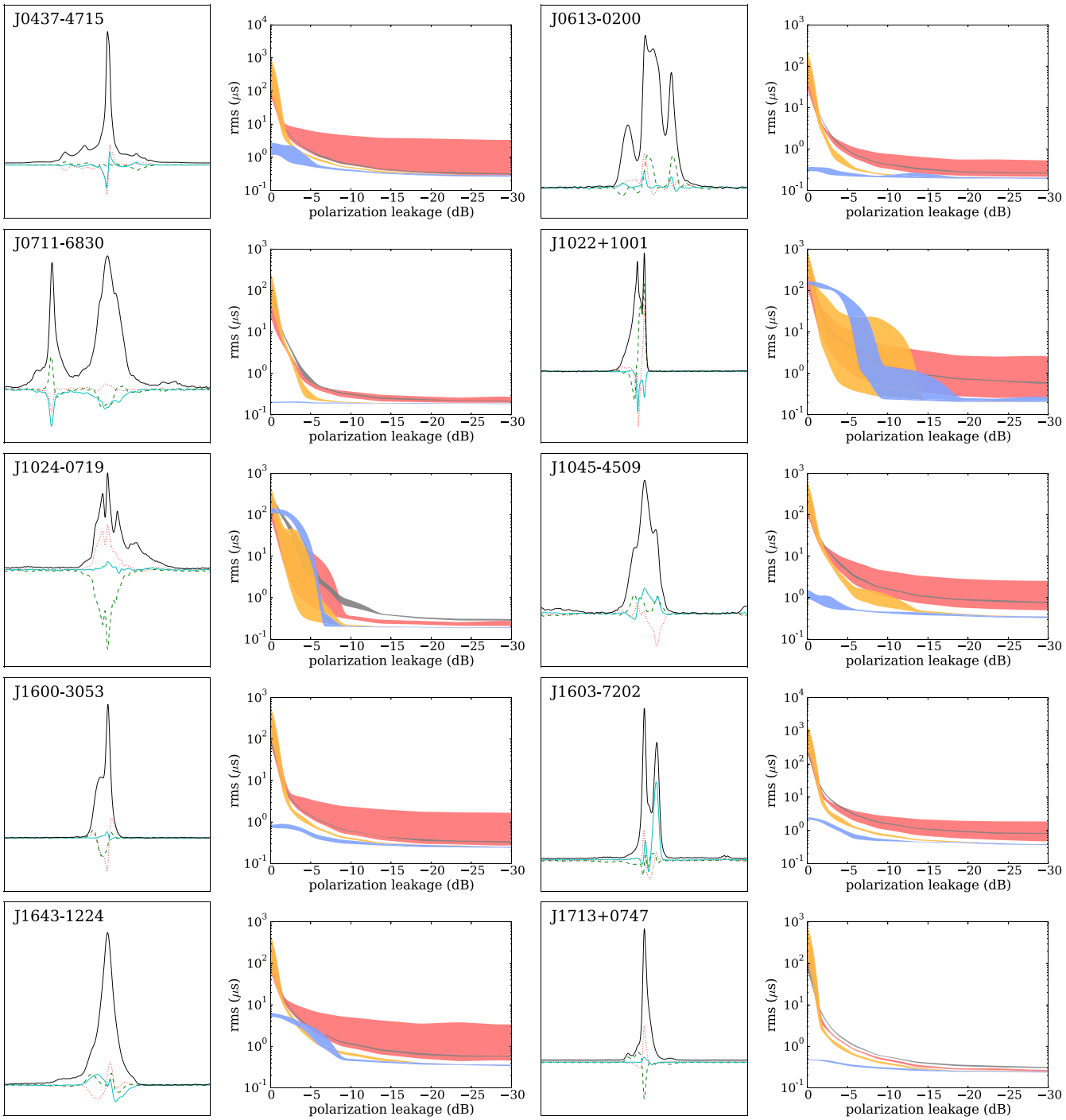

Figure 6. ToA rms noise from simulation of various MSPs. The first and third columns are the Stokes parameters of the ideal profile: I (black solid), Q (green dashed), U (red dotted), and V (cyan solid). The second and fourth columns show ToA rms noise (μs) as a function of intrinsic polarization leakage when using total intensity (red, no border), invariant interval (grey, dashed border), and matrix template matching (full calibration: orange, dotted border; gain calibration: blue, dot–dashed border) methods on the profile. The width of the lines shows the effect polarization calibration error has on the rms; a polarization calibration error from 0 to 15 per cent was used. These simulations use a fractional integration time of 0.01 which would produce an ideal S/N of 100. Plots continue in Fig. 7.

therefore further reduces the observed S/N of the calibrated profile. Adding polarization calibration error reduces the intrinsic polarization leakage, leading to an increase in the observed S/N. There is potential use for the total intensity method at high intrinsic polarization leakage when only using a 'gain' calibration. Needless to say, this regime should be avoided and this sets a maximum limit on the allowable intrinsic polarization leakage to around −5 dB.

Fig. 9 shows the residual timing rms of J1603−7202 as a function of S/N and $\mathrm{IXR_J}$ using a calibration error of 5 per cent. For a given integration time, the achievable ToA rms noise is dependent on the system polarization value, e.g. in simulation of J1603−7202 for $\tau_{\mathrm{int}} = 0.1$

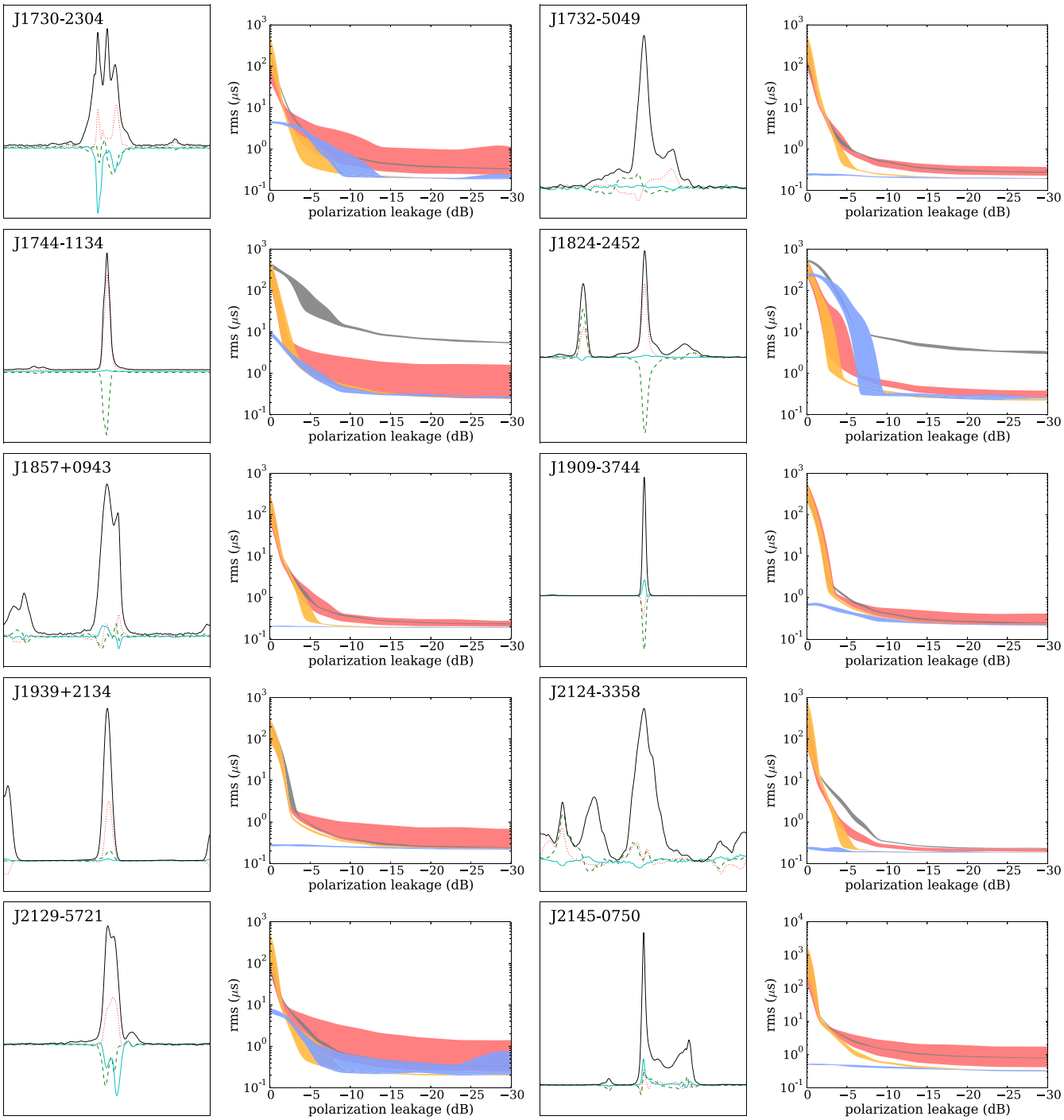

Figure 7. Continuation of Fig. 6, see that figure for description.

a system with −25 dB intrinsic polarization leakage can achieve a ToA rms in the timing residuals of around 300 ns compared to 3000 ns with a −5 dB intrinsic polarization leakage system. This variation due to intrinsic polarization leakage can be better seen in Fig. 10, which shows the residual rms as a function of integration length, for a range of intrinsic polarization leakage values. The rms will continue to decrease as the integration time increases. The system intrinsic polarization leakage sets the required integration time to achieve a desired rms. In Section 4, we discuss the importance of Fig. 10 in optimizing science return when there is limited available observing time.

4 DISCUSSION

Gravitational wave detection using high-precision timing of MSPs constitutes a key science project for the SKA. This imposes a requirement on the polarization specifications. In Cordes et al. (2004), a case is presented which sets the required polarization purity level to −40 dB to

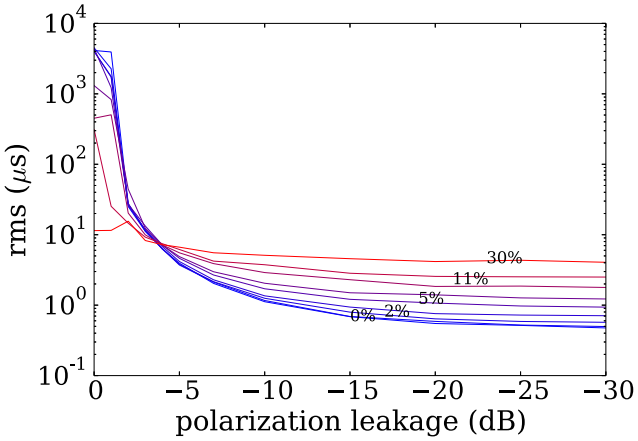

Figure 8. ToA rms noise using the total intensity method as a function of intrinsic polarization leakage for J1603−7202. Lines cover a range of polarization calibration errors from 0 per cent (blue) to 27 per cent (red). A normalized integration time of 0.01 was used for all the lines. A counter-intuitive effect occurs when the intrinsic polarization leakage is high, where the rms noise becomes inversely proportional to the calibration error because calibration errors improve the condition of the calibration matrix $\hat{\mathbf{M}}_{\rm sys}$.

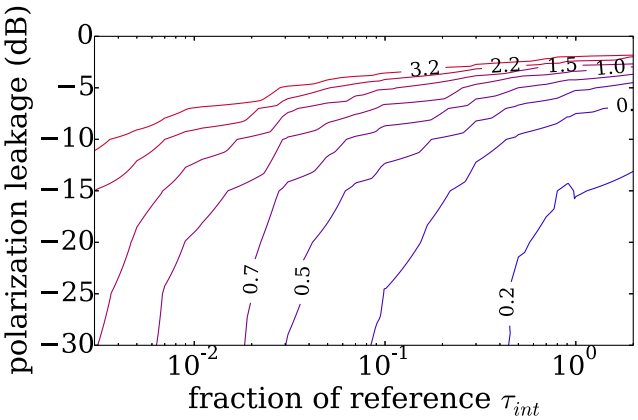

Figure 9. Contour plot of ToA rms noise (μs) using matrix template matching as a function of intrinsic polarization leakage and integration time for PSR J1603−7202. Integration time is a fraction of the reference integration time, see Section 1.3.

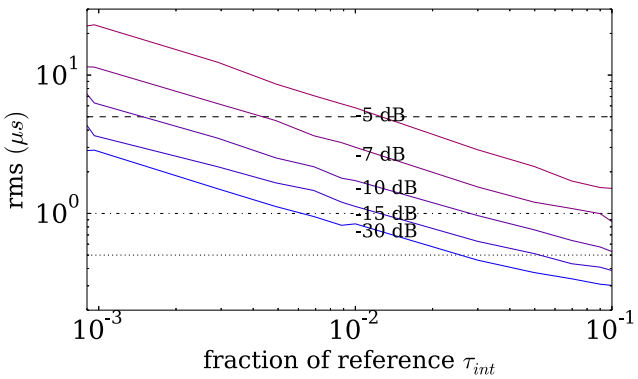

Figure 10. ToA rms noise of PSR J1603−7202, using the matrix template matching method, as a function of integration lengths for a range of intrinsic polarization leakage values. Horizontal lines indicate rms thresholds: 0.5 μs (dotted), 1 μs (dot–dashed), and 5 μs (dashed).

accomplish the SKA pulsar key science goals. This polarization purity value is different from what we have defined as polarization purity; it is a measure of the final, calibrated Stokes data and not a specification of the front-end design as we have considered here.

Fig. 10 shows that for a given intrinsic polarization leakage, a desired timing residual rms can be achieved with sufficient observing time. This, of course, ignores the other systematic effects that are part of a timing observation and does not include the additional sensitivity modulation of the primary beam shape. We have only focused on intrinsic polarization leakage, which is an effect on any feed design. The main issue is that the intrinsic polarization leakage has a strong effect on the required observation time, which is a limited commodity. For our simulation of MSP J1603−7202 in Fig. 10, the difference in required observing time to achieve a desired rms noise at −15 dB compared

Table 1. Fractional improvement in ToA rms noise between two IXR_J values for the simulated MSPs using the matrix template method. Percent change is computed as $\Delta_{ToA} = 100(rms_i - rms_f)/rms_i$, where rms_i is the initial (lower) IXR_J ToA rms noise and rms_f is the final (higher) IXR_J ToA rms noise. These simulations used a fractional integration length of 0.01, which is an ideal SNR of 100. The reported rms values have an uncertainty of ∼1 per cent set by the number of ToA simulations ($n = 5000$). The last rows of the table are the average ToA rms noise percent improvement and minimum/maximum range.

Pulsar	rms (ns) $IXR_J = 10$ dB	Δ_{ToA} (per cent) 10 dB → 20 dB	rms (ns) $IXR_J = 20$ dB	Δ_{ToA} (per cent) 20 dB → 30 dB	rms (ns) $IXR_J = 30$ dB	Δ_{ToA} (per cent) 30 dB → 40 dB	rms (ns) $IXR_J = 40$ dB
J0437−4715	545	43.1	310	9.4	281	3.2	272
J0613−0200	256	19.9	205	2.5	200	0.5	199
J0711−6830	202	7.9	186	0.5	185	0.0	185
J1022+1001	294	24.5	222	5.0	211	0.0	211
J1024−0719	217	11.1	193	1.6	190	1.1	188
J1045−4509	657	41.6	384	11.2	341	4.1	327
J1600−3053	445	38.7	273	9.2	248	2.0	243
J1603−7202	755	43.7	425	11.1	378	4.5	361
J1643−1224	704	44.0	394	10.9	351	1.7	345
J1713+0747	419	37.5	262	9.2	238	1.7	234
J1730−2304	336	40.2	201	3.5	194	0.5	193
J1732−5049	247	18.2	202	4.0	194	0.5	193
J1744−1134	463	37.1	291	9.6	263	1.9	258
J1824−2452	377	33.7	250	6.8	233	0.9	231
J1857+0943	211	8.1	194	1.5	191	0.5	190
J1909−3744	356	35.1	231	5.6	218	2.8	212
J1939+2134	354	33.9	234	5.6	221	1.8	217
J2124−3358	201	7.5	186	1.1	184	0.5	183
J2129−5721	274	22.6	212	3.8	204	2.0	200
J2145−0750	398	35.9	255	6.7	238	0.8	236
Average		29.2		6.0		1.6	
Range		7–44		1–11		0–4	

to −30 dB is a factor of 1.5. With limited available observing time, we would like to set an upper limit on the intrinsic polarization leakage above which it is no longer optimal to be using observation time on a measurement. Carozzi et al. (2009) and Sutinjo & Hall (2013) show the $IXR_{J,dB}$ for typical feeds to be somewhere between 30 and 66 dB at boresight. We see that observing with an intrinsic polarization leakage of −15 dB implies at least a 50 per cent increase in observing time compared to that of a typical feed. A high intrinsic polarization leakage is not a design issue for a 'classic' single pixel dish system, where a low intrinsic polarization leakage can be achieved when observing a source on axis. This is not the case with AAs, PAFs, and multi-beaming with single pixel dishes. In these cases, the source will likely not be located in the optimal intrinsic polarization leakage region of the beam. For AAs, a source will rarely, if ever, be on axis. Returning to the example beams in Carozzi et al. (2009) and Sutinjo & Hall (2013), we see that the polarization leakage values can quickly increase to above −10 dB away from zenith. This effectively limits the declination range of sources, depending on the array latitude, for pulsar timing.

From our simulation, we see there is an intrinsic polarization leakage lower limit on feed design at which point there is minimal return in terms of reducing the timing residual rms with further engineering investment, for a given integration time. As there is a cost to every incremental improvement in IXR, we would like to present our simulation results in terms scientific return for marginal improvements in engineering specifications. In an effort to create a meaningful engineering intrinsic polarization leakage lower limit, Table 1 lists the fractional improvement in ToA rms noise for different IXR values. We have picked a typical S/N ($\tau_{int} = 0.01$) for a timing observation. Columns 2, 4, 6, and 8 are the timing residual rms for each MSP at $IXR_J = 10, 20, 30, 40$ dB, respectively. Columns 3, 5, and 7 are the percentage change in the rms with the changes in IXR. This table shows the diminishing marginal utility of improving IXR for the benefit of decreasing the ToA rms noise. There is, on average, a 29 per cent improvement in the rms when improving the IXR_J from 10 to 20 dB, but can vary significantly with profile shape. For example, timing of J0711–6830 is largely unaffected by improvements in IXR, while timing of J1603–7202 improves with each increase in IXR. Going from 20 to 30 dB, there is a small improvement, but going above 30 dB provides essentially no improvement. This indicates that for a feed with $IXR_{J,dB} > 30$ dB, there is limited fractional improvement in pulsar timing capabilities. It may be worth considering that low intrinsic polarization leakage across the FoV may be preferable to optimizing for minimal intrinsic polarization leakage around boresight.

5 CONCLUSION

On the pathway towards the SKA, a number of AAs, dishes, and PAFs are being developed as precursor instruments. As pulsar timing is a key science project, design of these instruments should take into account the intrinsic polarization leakage specification we have presented in this paper.

There is a relative increase in required integration time as a function of the feed IXR, as seen in Fig. 10. At high intrinsic polarization leakage, this can make the required integration time inefficiently long.

We have shown that there are diminishing returns (Table 1) on building feed systems which have intrinsic polarization leakage below −30 dB in the direction of observation. Achieving this intrinsic polarization leakage limit should be easily affordable for single pixel dishes on axis, where the leakage is at a minimum. However, AAs, PAFs, and multi-beam systems, where observations are not always made in the direction of minimum leakage, could have limited use for pulsar timing if intrinsic polarization leakage is not taken into account while developing the feed system. The complex AA and PAF beams with sharp, frequency-dependent structure lead to regions of high intrinsic polarization leakage.

Given the effect of intrinsic polarization leakage on pulsar timing and a costing model for a feed design, a desirable optimization could be to maximize the average IXR across the intended usable FoV for the element and not just in the direction of boresight.

The calibratability of an array has a key effect on timing as we have shown with the idealized 'gain' calibration technique against the more realistic 'full' calibration. Beyond this work, there is scope for additional work on effect of calibration on timing. Additionally, the matrix template matching method should be extended to account for the covariances between the Stokes parameters induced by poorly conditioned calibration matrices.

Ideally, we can further refine these values on precursor instruments. The MeerKAT, KAT-7, ASKAP, and APERTIF arrays will provide a platform to study dish array polarization effects with multi-beam feeds and PAFs. LOFAR and MWA, though not ideal for pulsar timing experiments due to the low observing frequencies, will be useful to study instrumental polarization in AAs. A study of these array polarization properties is necessary to assure the SKA science specifications can be met for pulsar timing.

ACKNOWLEDGEMENTS

This work is based upon research supported by the South African Research Chairs Initiative of the Department of Science and Technology and National Research Foundation.

REFERENCES

Britton M. C., 2000, ApJ, 532, 1240
Carozzi T. D., Woan G., 2011, IEEE Trans. Antennas Propag., 59, 2058
Carozzi T. D., Woan G., Maaskant R., 2009, in Torchinsky S. A., van Ardenne A., van den Brink-Havinga T., van Es A. J. J., Faulkner A. J., eds., Proc. Wide Field Astronomy & Technology for the Square Kilometre Array, Polarization Diversity for SKA Wide-Field Polarimetry. European Commission Framework Programme 6, p. 17
Cordes J. M., Kramer M., Lazio T. J. W., Stappers B. W., Backer D. C., Johnston S., 2004, New Astron. Rev., 48, 1413
Hamaker J. P., 2000, A&AS, 143, 515
Hamaker J. P., Bregman J. D., Sault R. J., 1996, A&AS, 117, 137
Han J. L., Demorest P. B., van Straten W., Lyne A. G., 2009, ApJS, 181, 557
Hobbs G. B., Edwards R. T., Manchester R. N., 2006, MNRAS, 369, 655
Hotan A. W., van Straten W., Manchester R. N., 2004, PASA, 21, 302
IEEE, 1998, IEEE Standard 211-1997, IEEE Standard Definitions of Terms for Radio Wave Propagation. IEEE
Janssen G. et al., 2015, Proc. Sci., Gravitational Wave Astronomy with the SKA. SISSA, Trieste, PoS(AASKA14)037
Lorimer D., 2005, Cambridge Observing Handbooks for Research Astronomers, Handbook of Pulsar Astronomy. Cambridge Univ. Press, Cambridge
Manchester R. N. et al., 2013, PASA, 30, 17
Smirnov O. M., 2011a, A&A, 527, A106
Smirnov O. M., 2011b, A&A, 527, A107
Sutinjo A. T., Hall P. J., 2013, IEEE Trans. Antennas Propag., 61, 2852
Taylor J. H., 1992, Phil. Trans. R. Soc. A, 341, 117
van Straten W., 2006, ApJ, 642, 1004
van Straten W., 2013, ApJS, 204, 13
van Straten W., Demorest P., Oslowski S., 2012, Astron. Res. Technol., 9, 237

This paper has been typeset from a TEX/LATEX file prepared by the author.